RESONANT INVERTER SUPPLIED INTERIOR PERMANENT MAGNET (IPM) MOTOR ROTOR POSITION INFORMATION EXTRACTION FROM THE RESONANT COMPONENT CURRENT

Mengesha Mamo
School of Electrical & Computer Engineering, Addis Ababa Institute of Technology, AAU
Corresponding Author's Email: mmamo2006@gmail.com

ABSTRACT

In this paper, rotor position in relation to the resonant frequency component current in the stator winding of DC-voltage link resonant inverter supplied Interior Permanent Magnet (IPM) motor has been developed. Six reference frames are used to relate the rotor position angle to the resonant frequency component current explicitly. Two reference frames are used at a time for each 60^0 sector of voltage vector. The relation has been simplified for easy implementation using microprocessors. The simulation result demonstrates that the technique is effective in extracting the rotor position information from the measured resonant frequency component current.

Keywords: IPM motor, Sensorless, Two reference frame, resonant frequency

INTRODUCTION

Permanent magnet (PM) electric motors are, in general, efficient compared to induction and DC motors, due to the absence of copper loss in the excitation circuit. PM motors can be Interior Permanent Magnet (IPM) or Surface Permanent Magnet (SPM) depending on the placement of the permanent magnets with respect to the rotor surface. In SPM motors, the magnets are placed on the surface of the rotor while in the IPM motors the permanent magnets are placed under the surface of the rotor.

Control of permanent magnet motor requires rotor position information for proper commutation of the inverter switches, so that the desired torque is produced to rotate the motor in the desired direction and speed. Traditionally, mechanical rotor position sensors are attached to the rotor shaft and used as rotor position information source. However, mechanical sensors are not reliable and constitute significant component of the drive cost [1]. Researchers have suggested and developed various methods of mechanical rotor position sensor elimination. Back Electromotive force (EMF) method, observer method, and high frequency current injection method [1] are most common in literature.

Back EMF and observer-based methods have difficulty in the lower speed range. This is because the EMF magnitude diminishes as speed approaches zero. The high frequency injection method, on the other hand, has difficulty in proper frequency selection; as it should normally be between the carrier frequency of the inverter and the fundamental frequency. If the injected frequency is close to the currier frequency, filtering the injected signal becomes difficult. On the other hand, if the injected signal is close to the fundamental frequency, it results in rippling torque. The additional power requirement is also further shortcomings of this method. IPM motors have saliency such that the inductance in the quadrature direction is larger than the inductance in the direct axis [1, 4].

In [4] the paper proposes and demonstrates the use of carrier frequency component current method (CFCM) for sensorless control of IPM motors. In the CFCM the redundant carrier frequency component current of sine-triangle modulated hard switched inverter and saliency of the IPM motor have been used as rotor position information source. Rotor information is extracted using two reference frames. As the switching frequency of hard switched inverters increase, switching loss and electromagnetic interference (EMI) increase [3]. In order to overcome these problems soft switching (switching while the voltage across or current through the switch is zero) known as resonant inverter has been introduced. DC-voltage link resonant inverters are the most common resonant inverters used in industry. However, sensorless control of IPM motors supplied by such inverters has not yet been reported.

In this work, DC-voltage link resonant inverter supplied IPM motors' rotor position extraction

technique from measured resonant frequency component current has been developed. IPM motors' saliency and the resonant frequency component current in the stator windings are used as rotor position information source. Three sets of reference frames are used to simplify the extraction of rotor position angle for implementation.

INDUCTANCE VARIATION WITH ROTOR POSITION

If the three-phase stator windings of an IPM motor are replaced by two-phase imaginary windings, one along phase-u axis (α-axis) and the other at 90^0 (β-axis) degrees ahead of phase-u axis, and the direct-axis of the rotor is at angle θ from the phase-u axis, the self inductance of the two windings can be expressed by equations (1a) and (1b) [4]. Similarly, if the three-phase winding is replaced by similar two-phase winding, one at 45^0 (α'-axis) and the other at 135^0 (β'-axis) from phase-u winding axis, the self inductance of the new windings can be shown to be as in Equ. (2a) and Equ. (2b).

$$L_{s\alpha}(\theta) = L_{sum} - L_{diff}\cos(2\theta) \quad (1a)$$

$$L_{s\beta}(\theta) = L_{sum} + L_{diff}\cos(2\theta) \quad (1b)$$

$$L_{s\alpha'}(\theta) = L_{sum} - L_{diff}\sin(2\theta) \quad (2a)$$

$$L_{s\beta'}(\theta) = L_{sum} + L_{diff}\sin(2\theta) \quad (2b)$$

Where; $L_{sum} = (\frac{L_d + L_q}{2})$ and $L_{diff} = \frac{L_q - L_d}{2}$

Where, L_d is the direct axis inductance and L_q is the quadrature axis inductance, θ is the angle between the rotor direct axis and the phase-u winding axis.

Therefore, if the inductance of the imaginary windings at the four axes are monitored the rotor position can easily be obtained from Equ. (3) [4].

$$\theta = \frac{1}{2}\tan^{-1}\left(\frac{L_{S\beta'} - L_{S\alpha'}}{L_{S\beta} - L_{S\alpha}}\right) \quad (3)$$

Similarly, various axes can be selected to simplify the rotor position angle expression in terms of the self-inductance values of imaginary windings at the axes. The general expression for self-inductance value at an x-axis, which is θ_x from phase-u axis, is expressed as in Equ. (4).

$$L_{sx}(\theta_x) = L_{sum} - L_{diff}\cos(2\theta + 2\theta_x) \quad (4)$$

The proper axes, with self inductance given by Equ. (4), for effectively extracting the rotor position from resonant frequency component currents are presented in the following section.

ROTOR POSITION ANGLE AND THE RESONANT CURRENT

The Resonant Voltage and Reference Frame Selection

In Fig. 1, an actively clamped resonant DC-link inverter is shown. The resonant inverter generates pulses at the resonant frequency across capacitor C_r [5].

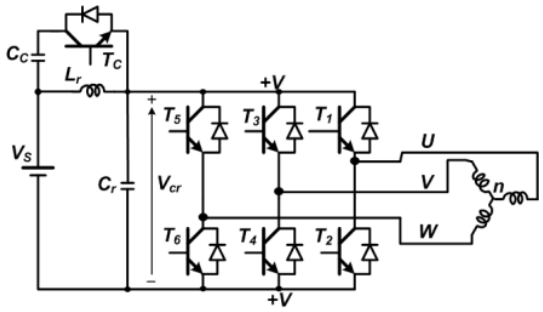

Fig. 1: Resonant Inverter supplying an IPM motor (Source: [5])

The voltage magnitude is controlled by the number of pulses, as opposed to the pulse width in PWM inverters. The natures of pulses during the possible switch combinations of Fig. 1 are demonstrated in Fig. 2.

In Fig. 2, column two, three, four, five, six and seven correspond to the voltage vectors generated in 0^0, 60^0, 120^0, 180^0, 240^0, 300^0 from phase-u axis. Corresponding to the six voltage vectors, the resonant frequency component voltage across the three-phase stator windings can be given as the second, third and fourth columns of *table-1*, where $\boldsymbol{V_m}$ and ω_r are the resonant frequency component peak voltage and the resonant frequency in rad/sec, respectively.

The three phase windings can be replaced by two imaginary phase windings supplied by voltages of equal magnitude, as shown in columns five and six, if the reference frames in the last column are used.

Therefore; reference frames given in the last column of table-1, are selected for the various sectors as follows.

For sector-1 45^0-135^0 and 105^0-195^0, for sector-2 105^0-195^0 and 165^0-195^0, for sector-3 165^0-255^0 and 225^0-315^0, for sector-4 225^0-315^0 and 285^0-15^0, for sector-5 285^0-15^0 and 345^0-75^0, and for sector-6 345^0-$75^0$and 45^0-135^0. Sectors one to sector six refers to space between two consecutive voltage vectors from left to right on Fig. 2. Note that, a voltage vector in a sector is generated by proper combination of the two adjacent voltage vectors.

Inductance Value at Selected Reference frames

The self inductance value of the imaginary windings at the six reference frames are given in Table-2, below. Note that all have the same form and are functions of the rotor position angle. The constant component of the self inductance value at the selected axes can be eliminated by combining two axes as shown in the last column of Table-2. Then, the adjacent two reference frames can be used to solve for the rotor position angle, as shown inTtable-3, if the inductance values at the corresponding four axes values are known.

Measurement of the inductance of the imaginary axes is not straight forward and this makes. use of the above expressions for rotor position angle determination a bit difficult. In the following sub-section indirect measurement of inductance value using the resonant frequency component current is developed.

Rotor Position angle Relation to Resonant Current

The voltage equations of the resonant frequency component in the imaginary windings can be used to relate the rotor position angle to the resonant current. The resistance of the imaginary coils is neglected compared to the inductive reactance, which is very high because of high frequency. It can be shown that the voltage equation of the imaginary windings at angle x and $x+90^0$ can be given by Equ. (5).

For non-singular inductance matrix in Equ. (5), the current can be solved for as in Equ. (6) which can be reduced to Equ. (7), below, for selected instants, instants at which the voltage v_x is at its positive peak. At this instant v_{x+90} is at its negative peak with magnitude equal to v_x. One can sum up Equ. (7a) and Equ. (7b), resulting in Equ. (8), for selected instants.

$$2\frac{v_x}{L_{sum}^2 - L_{diff}^2}[L_{diff}\cos(2\theta + 2x)] = \frac{di_{x+90}}{dt} + \frac{di_x}{dt} \qquad (8)$$

For inductive impedance, where the resistance is neglected, the differential currents in Equ. (8) can also be approximated to be at their peak values at the instant v_x is at its peak value. Therefore, the peak values of the currents carry the rotor position information.

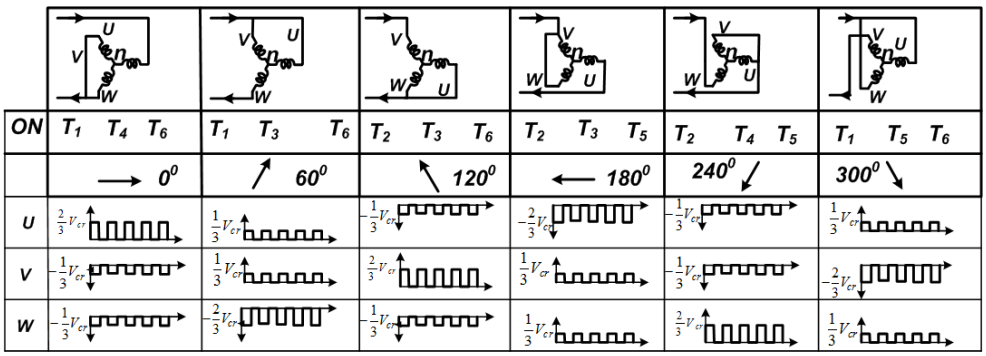

Fig. 2: Space-vector modulation, non-zero and non-short-circuit switch positions

Table-1: Resonant Frequency Component voltage in the three-phase stator

	u_r	v_r	w_r	*Voltage across the two imaginary windings*		*Reference Frame*
$360^0/0^0$	$\frac{2}{3}V_m\sin(\omega_r t)$	$-\frac{1}{3}V_m\sin(\omega_r t)$	$-\frac{1}{3}V_m\sin(\omega_r t)$	$v_{45}=\frac{1}{\sqrt{2}}V_m\sin(\omega_r t)$	$v_{135}=-\frac{1}{\sqrt{2}}V_m\sin(\omega_r t)$	45^0-135^0
60^0	$\frac{1}{3}V_m\sin(\omega_r t)$	$\frac{1}{3}V_m\sin(\omega_r t)$	$-\frac{2}{3}V_m\sin(\omega_r t)$	$v_{105}=\frac{1}{\sqrt{2}}V_m\sin(\omega_r t)$	$v_{195}=-\frac{1}{\sqrt{2}}V_m\sin(\omega_r t)$	105^0-195^0
120^0	$-\frac{1}{3}V_m\sin(\omega_r t)$	$\frac{2}{3}V_m\sin(\omega_r t)$	$-\frac{1}{3}V_m\sin(\omega_r t)$	$v_{165}=\frac{1}{\sqrt{2}}V_m\sin(\omega_r t)$	$v_{255}=-\frac{1}{\sqrt{2}}V_m\sin(\omega_r t)$	165^0-255^0
180^0	$-\frac{2}{3}V_m\sin(\omega_r t)$	$\frac{1}{3}V_m\sin(\omega_{rf} t)$	$\frac{1}{3}V_m\sin(\omega_{rf} t)$	$v_{-135}=\frac{1}{\sqrt{2}}V_m\sin(\omega_r t)$	$v_{-45}=-\frac{1}{\sqrt{2}}V_m\sin(\omega_r t)$	225^0-315^0
240^0	$-\frac{1}{3}V_m\sin(\omega_r t)$	$-\frac{1}{3}V_m\sin(\omega_r t)$	$\frac{2}{3}V_m\sin(\omega_r t)$	$v_{-75}=\frac{1}{\sqrt{2}}V_m\sin(\omega_r t)$	$v_{15}=-\frac{1}{\sqrt{2}}V_m\sin(\omega_r t)$	285^0-15^0
300^0	$\frac{1}{3}V_m\sin(\omega_r t)$	$-\frac{2}{3}V_m\sin(\omega_r t)$	$\frac{1}{3}V_m\sin(\omega_r t)$	$v_{-15}=\frac{1}{\sqrt{2}}V_m\sin(\omega_r t)$	$v_{75}=-\frac{1}{\sqrt{2}}V_m\sin(\omega_r t)$	345^0-75^0

Table 2: Self inductance at the selected axes

Axis	*Self inductance*		*Axis*	*Self inductance*	*Variable part of inductance*
45^0	$L_{s45}(\theta)=L_{sum}-L_{diff}\cos(2\theta+90)$		135	$L_{s135}(\theta)=L_{sum}-L_{diff}\cos(2\theta+90+180)$	$L_{s45}(\theta)-L_{s135}(\theta)=2L_{diff}\sin(2\theta)$
105^0	$L_{s105}(\theta)=L_{sum}-L_{diff}\cos(2\theta+210)$		195^0	$L_{s195}(\theta)=L_{sum}-L_{diff}\cos(2\theta+210+180)$	$L_{s105}(\theta)-L_{s195}(\theta)=-L_{diff}\cos(2\theta+210)$
165^0	$L_{s165}(\theta)=L_{sum}-L_{diff}\cos(2\theta+330)$		255^0	$L_{s135}(\theta)=L_{sum}-L_{diff}\cos(2\theta+330+180)$	$L_{s165}(\theta)-L_{s135}(\theta)=-2L_{diff}\cos(2\theta+330)$
225^0	$L_{s-135}(\theta)=L_{sum}-L_{diff}\cos(2\theta+90)$		315^0	$L_{s-45}(\theta)=L_{sum}-L_{diff}\cos(2\theta+90+180)$	$L_{s-135}(\theta)-L_{s-45}(\theta)=2L_{diff}\sin(2\theta)$
285^0	$L_{s-75}(\theta)=L_{sum}-L_{diff}\cos(2\theta+210)$		15^0	$L_{s15}(\theta)=L_{sum}-L_{diff}\cos(2\theta+210+180)$	$L_{s-75}(\theta)-L_{s15}(\theta)=-L_{diff}\cos(2\theta+210)$
345^0	$L_{s-15}(\theta)=L_{sum}-L_{diff}\cos(2\theta+330)$		75^0	$L_{s75}(\theta)=L_{sum}-L_{diff}\cos(2\theta+330+180)$	$L_{s-15}(\theta)-L_{s75}(\theta)=-2L_{diff}\cos(2\theta+330)$

Table 3: Rotor position extraction from self inductance of imaginary windings

Sector	Rotor angle equation	Definition		Sector	Rotor angle equation	Definition
I	$\theta=\frac{1}{2}\tan^{-1}(\frac{\cos(210^0)}{x_1+\sin(210^0)})$	$x_1=\frac{L_{S105}-L_{S195}}{L_{S45}-L_{S135}}$		IV	$\theta=\frac{1}{2}\tan^{-1}(\frac{\cos(210^0)}{x_4+\sin(210^0)})$	$x_4=\frac{L_{S-75}-L_{S15}}{L_{S-135}-L_{S-45}}$
II	$\theta=\frac{1}{2}[\tan^{-1}(\frac{\cos(120^0)-x_2}{\sin 120^0})-120^0]$	$x_2=\frac{L_{S165}-L_{S135}}{L_{S105}-L_{S195}}$		V	$\theta=\frac{1}{2}[\tan^{-1}(\frac{\cos(120^0-x_5)}{\sin(120^0)})-120]$	$x_5=\frac{L_{S-15}-L_{S75}}{L_{S-75}-L_{S15}}$
III	$\theta=\frac{1}{2}\tan^{-1}(\frac{\cos(330^0)}{x_3+\sin(330^0)})$	$x_3=\frac{L_{S165}-L_{S135}}{L_{S-135}-L_{S-45}}$		VI	$\theta=\frac{1}{2}\tan^{-1}(\frac{\cos(330^0)}{x_6+\sin(330^0)})$	$x_6=\frac{L_{S-15}-L_{S75}}{L_{S45}-L_{S135}}$

$$\begin{bmatrix} v_x \\ v_{x+90^0} \end{bmatrix}=\begin{bmatrix} L_{sum}-L_{diff}\cos(2\theta+2x) & L_{diff}\sin(2\theta+2x) \\ L_{diff}\sin(2\theta+2x) & L_{sum}+L_{diff}\cos(2\theta+2x) \end{bmatrix}\frac{d}{dt}\begin{bmatrix} i_x \\ i_{x+90^0} \end{bmatrix} \tag{5}$$

$$\frac{d}{dt}\begin{bmatrix} i_x \\ i_{x+90^0} \end{bmatrix}=\frac{1}{L_{sum}^2-L_{diff}^2}\begin{bmatrix} L_{sum}+L_{diff}\cos(2\theta+2x) & -L_{diff}\sin(2\theta+2x) \\ -L_{diff}\sin(2\theta+2x) & L_{sum}-L_{diff}\cos(2\theta+2x) \end{bmatrix}\begin{bmatrix} v_x \\ v_{x+90^0} \end{bmatrix} \tag{6}$$

$$\frac{v_x}{L_{sum}^2-L_{diff}^2}[L_{sum}+L_{diff}\cos(2\theta+2x)]+\frac{v_x}{L_{sum}^2-L_{diff}^2}[L_{diff}\sin(2\theta+2x)]=\frac{di_x}{dt} \tag{7a}$$

$$\frac{v_x}{L_{sum}^2-L_{diff}^2}[-L_{diff}\sin(2\theta+2x)]+\frac{v_x}{L_{sum}^2-L_{diff}^2}[-L_{sum}+L_{diff}\cos(2\theta+2x)]=\frac{di_{x+90}}{dt} \tag{7b}$$

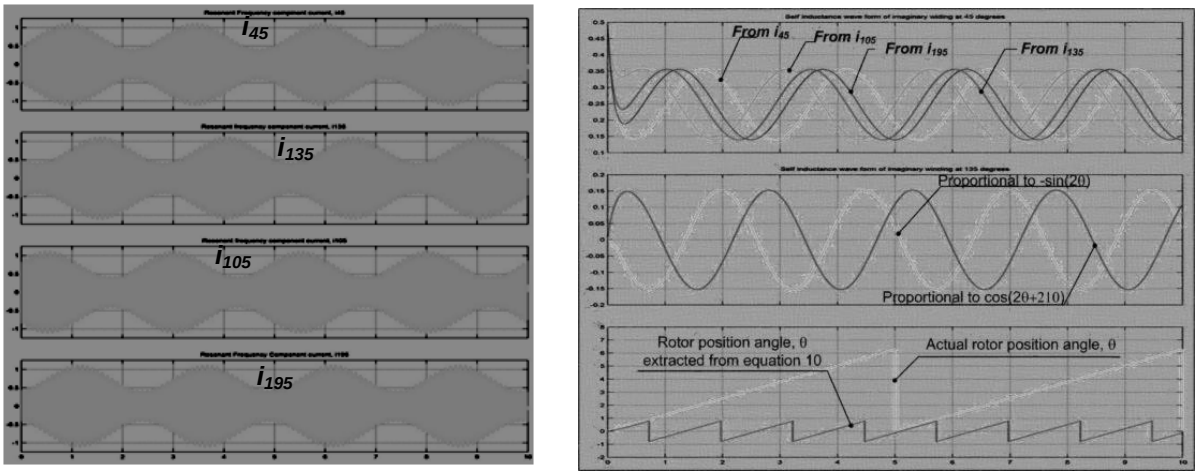

(a) (b)

Fig. 3: Rotor position extractions

(a) Resonant frequency current modulated with rotor position angle

(b) Upper inductance (Equ. (8) for i_{45}, i_{135}, i_{105}, i_{195}) of imaginary windings, middle constant part removed (Equ. (9)) and the last rotor position extracted per Equ. (10) and actual rotor position angle.

Furthermore, the peak of the currents is proportional to the integral of the absolute values of the currents. That is, $\int_0^T |i_x| dt$ is proportional to peak of $\boldsymbol{i_x}$.

The rotor position information while the voltage vector is in sector-1:

$\int_0^T |i_{45}| dt$ is proportional to the peak of $\frac{di_{45}}{dt}$ while $\int_0^T |i_{135}| dt$ is proportional to the peak of $\frac{di_{135}}{dt}$. Similarly, $\int_0^T |i_{105}| dt$ is proportional to the peak of $\frac{di_{105}}{dt}$ while $\int_0^T |i_{195}| dt$ is proportional to the peak of $\frac{di_{195}}{dt}$. From this argument Equ. (9) can be derived, where *K* is a constant.

$$\int_0^T |i_{45}| dt - \int_0^T |i_{135}| dt = KL_{diff} \sin 2\theta \tag{9a}$$

$$\int_0^T |i_{105}| dt - \int_0^T |i_{195}| dt = KL_{diff} \cos(2\theta + 210) \tag{9b}$$

From these two equations the rotor position angle, $\boldsymbol{\theta}$ can be solved resulting in Equ. (10). The expression for the rotor angle position in the other sectors can be written similarly using the symmetry of the three-phase motors.

Integrations of the resonant frequency component currents, shown in the equation, need not be evaluated. Instead, they can be estimated by moving average of absolute value of the currents over one period. This simplifies the implementation of the technique.

$$\theta = \frac{1}{2} \tan^{-1}\left(\frac{\cos(210^0)}{\frac{\int_0^T |i_{105}| dt - \int_0^T |i_{195}| dt}{\int_0^T |i_{45}| dt - \int_0^T |i_{135}| dt} + \sin(210^0)}\right) \tag{10}$$

Equ. (10) doesn't incorporate the motor parameters also. This results in the parameter insensitivity of the rotor position extraction technique.

SIMULATION RESULT

The rotor position extraction technique proposed is simulated for an IPM motor with L_d/L_q ratio of 2. The resonant frequency is selected to be 20 kHz. In Fig. 3a, resonant component current resolved to the axes at 45^0, 135^0, 105^0, and 195^0 are shown (from top to down) as the rotor rotates for two cycles. In (b) the upper curves demonstrates the self-inductance curve, Equ. (7), while the middle curve is from Equ. (9a) and (9b). The last two curves are the actual rotor position angle and the extracted rotor position angle. The actual rotor position angle varies between 0 and 2π while the extracted rotor position angle value varies between $\pi/4$ and $-\pi/4$.

CONCLUSION

This work has demonstrated that the rotor position information can be extracted from the saliency of an IPM motor and resonant frequency component current in the stator winding. The extraction technique is easy for practical implementation and is insensitive to parameter variation.

Probable challenge in the implementation is the need for two analogue-to-digital converters of high sampling frequency to sample the currents of two-phases. The sampling frequency should be at least two times the resonant frequency.

Future Work

The researchers are working on the complete modeling and simulation with sensorless feedback speed control of IPM motor to report in the final paper plus its experimental investigation.

REFERENCES

[1] Devid Saltiveri, Antony Arias "*Sensorless Control of Surface Mounted Permanent Magnet Synchronous Motors Using Matrix Converters*", Electric Power Quality and Utilization Journal Vol. X, No. 1, 2006

[2] Jung-Ik Ha, and others, "*Sensorless Rotor Position Estimation of an Interior Permanent-Magnet Motor From Initial States*", IEEE Transaction on Industry Application, Vol. 39, NO. 3, May/June 2003 761

[3] Fang Z. Peng and Donald J. Adams, "*An auxiliary Quasi-Resonant Tank Soft-Switching Inverter*", Oak Ridge National Laboratory, Oak Ridge Tennessee 37831-8038

[4] Mengesha Mamo &others, "*Novel Rotor Position Extraction Based on Carrier Frequency Component Method (CFCM) Using Two Reference Frames for IPM Drives*", IEEE transaction on Industrial Electronics, Vol. 52 No. 2, April 2005.

[5] Zhenyue Hong, "*DC-voltage link resonant inverters*", Department of Electrical and Electronic Engineering University of Canterbury, New Zealand

[6] Kalyan Kumar Halder, Naruttam Kumar Roy and B.C. Ghosh, "*Position Sensorless Control for an Interior Permanent Magnet Synchronous Motor SVM Drive with ANN Based Stator Flux Estimator*" International Journal of Computer and Electrical Engineering, Vol. 2, No. 3, June, 2010